Eur Biophys J (2010) 39:263–276
DOI 10.1007/s00249-009-0530-1

ORIGINAL PAPER

Biophysical studies of the interactions between the phage ϕKZ gp144 lytic transglycosylase and model membranes

Isabelle Cloutier · Catherine Paradis-Bleau · Anne-Marie Giroux · Xavier Pigeon · Marjolaine Arseneault · Roger C. Levesque · Michèle Auger

Received: 23 June 2009 / Revised: 14 July 2009 / Accepted: 22 July 2009 / Published online: 8 August 2009

Abstract The use of naturally occurring lytic bacteriophage proteins as specific antibacterial agents is a promising way to treat bacterial infections caused by antibiotic-resistant pathogens. The opportunity to develop bacterial resistance to these agents is minimized by their broad mechanism of action on bacterial membranes and peptidoglycan integrity. In the present study, we have investigated lipid interactions of the gp144 lytic transglycosylase from the *Pseudomonas aeruginosa* phage ϕKZ. Interactions with zwitterionic lipids characteristic of eukaryotic cells and with anionic lipids characteristic of bacterial cells were studied using fluorescence, solid-state nuclear magnetic resonance, Fourier transform infrared, circular dichroism, Langmuir monolayers, and Brewster angle microscopy (BAM). Gp144 interacted preferentially with anionic lipids, and the presence of gp144 in anionic model systems induced membrane disruption and lysis. Lipid domain formation in anionic membranes was observed by BAM. Gp144 did not induce disruption of zwitterionic membranes but caused an increase in rigidity of the lipid polar head group. However, gp144 interacted with zwitterionic and anionic lipids in a model membrane system containing both lipids. Finally, the gp144 secondary structure was not significantly modified upon lipid binding.

Keywords Antimicrobials · Endolysins · Infrared · NMR · Fluorescence · Spectroscopy

I. Cloutier · A.-M. Giroux · X. Pigeon · M. Arseneault · M. Auger (✉)
Département de Chimie, Regroupement Québécois de Recherche sur la Fonction, la Structure et l'Ingénierie des Protéines (PROTEO), Centre de Recherche sur les Matériaux Avancés (CERMA), Université Laval, Quebec, QC G1V 0A6, Canada
e-mail: michele.auger@chm.ulaval.ca

C. Paradis-Bleau · R. C. Levesque
Département de Biologie Médicale, PROTEO, Institut de Biologie Intégrative et des Systèmes (IBIS), Université Laval, Quebec, QC G1V 0A6, Canada

Introduction

Since 1960, the increase in bacterial resistance to traditional antibiotics has become an important problem, and it is imperative to find creative alternative strategies to prevent and fight bacterial infections (Normark and Normark 2002). Bacteriophages have been viewed as a source of potential antibacterial therapeutics (Projan 2004; Thiel 2004). These bacterial viruses produce large amounts of lytic proteins having antibacterial activity. Double-stranded DNA phages typically produce soluble muralytic enzymes known as endolysins. These enzymes hydrolyze the cell wall peptidoglycan layer that is unique to bacteria. The cell wall confers morphology and integrity to the bacterial cell and is essential for growth and survival (Fischetti 2001, 2005). Double-stranded DNA phage endolysins usually require a small membrane protein or holin that permeates the bacterial cytoplasmic membrane, allowing the endolysin to access the periplasmic peptidoglycan (Ramanculov and Young 2001; Young et al. 2000).

Pseudomonas aeruginosa is a Gram-negative bacterium responsible for several systemic infections, particularly lung infections in cystic fibrosis and immunosuppressed patients (Davies 2002). This organism is one of the most difficult to eradicate in nosocomial infections due to

resistance to most classes of antibiotics (Davies 2002). The bacteriophage ϕKZ has been shown to efficiently infect and lyse *P. aeruginosa* strains isolated from human infections (Ackermann 2003). ϕKZ encodes two endolysin homologues, gp144 and gp188 (Briers et al. 2007; Mesyanzhinov et al. 2002; Paradis-Bleau et al. 2007). In this study, we have focused on gp144, which has been shown to adopt mainly an α-helical structure (Fokine et al. 2008). This enzyme has a molecular weight of 28.8 kDa and an isoelectric point of 9.10. It also has two functional domains, an N-terminal domain allowing binding to the peptidoglycan and a C-terminal domain responsible for the lytic transglycosylase activity (Briers et al. 2007). However, exhaustive bioinformatics analysis did not identify any typical holin-encoding gene in the ORFs of the ϕKZ genome sequence (Paradis-Bleau et al. 2007). Few studies report bacteriophages that code for endolysins without a holin (Borysowski et al. 2006; Morita et al. 2001). More specifically, it has been shown that overexpression of a specific endolysin in *Escherichia coli* can enhance cell lysis without the holin protein or the N-terminal signal sequence (Morita et al. 2001). Some endolysins have also been shown to be translocated to the bacterial periplasm by the host Sec-dependent secretion system through typical N-terminal signal sequence (Sao-José et al. 2000) or signal-arrest-release (SAR) sequence (Xu et al. 2004). In the SAR system, triggering of the holin at the programmed lysis time was suggested to facilitate the release of the endolysin from the membrane.

Bioinformatics analysis performed on gp144 did not identify any N-terminal signal sequence (Paradis-Bleau et al. 2007). However, the gp144 lytic transglycosylase enzyme was shown to have in vitro antibacterial activity against *E. coli* and *P. aeruginosa* cells (Paradis-Bleau et al. 2007) and to interact with anionic lipids (Paradis-Bleau et al. 2007). Gp144 contains a weakly positively charged region in the N-terminal domain, followed by a hydrophobic α-helical region. It has been hypothesized that these regions may allow gp144 to interact and permeabilize bacterial membranes (Paradis-Bleau et al. 2007).

The goal of the present study was to understand how gp144 interacts with anionic bacterial membranes to access peptidoglycan. More specifically, the interactions between gp144 and model membranes were investigated using a variety of biophysical techniques, including fluorescence, solid-state nuclear magnetic resonance (NMR) and Fourier transform infrared (FTIR) spectroscopy, circular dichroism, Langmuir monolayers, and Brewster angle microscopy (BAM). With the aim of better characterizing gp144 and its interaction with bacterial membranes, zwitterionic (phosphatidylcholine) and anionic (phosphatidylglycerol) lipids were used to mimic eukaryotic and bacterial membranes, respectively.

Materials and methods

gp144 and lipids

The gp144 protein was produced as described by Paradis-Bleau et al. (2007). The electrostatic potential on the solvent-accessible surface of the 3D structure of gp144 (PDB code 3BKH) was calculated using PBEQ-Solver (Sunhwan et al. 2008). 1-Palmitoyl-2-oleoyl-*sn*-glycero-3-phosphocholine (POPC), 1-palmitoyl-2-oleoyl-*sn*-glycero-3-phosphoglycerol (POPG), 1,2-dimyristoyl-*sn*-glycero-3-phosphocholine (DMPC), DMPC deuterated on both acyl chains (DMPC-d_{54}), and 1,2-dimyristoyl-*sn*-glycero-3-phosphoglycerol (DMPG) were purchased from Avanti Polar Lipids (Alasbaster, AL, USA) and used without further purification. Calcein and the salts used for the preparation of the buffer solutions were purchased from Sigma Aldrich (Milwaukee, WI, USA) and used without further purification.

Fluorescence spectroscopy

For calcein release assays, a calcein solution was prepared by dilution of calcein in an internal buffer (100 mM HEPES, 30 mM NaCl, and 5 mM EDTA) to obtain a calcein concentration of 80 mM at pH 7.4. A defined amount of lipids was diluted in 1 ml of the calcein-containing buffer. After five freeze/thaw cycles, the lipid dispersions were extruded 11 times using a 0.1-μm polycarbonate filter according to the Avanti Mini-Extruder procedures (Avanti Polar Lipids, Alabaster, AL, USA). Vesicles were separated from free calcein by Sephadex G-50 exclusion chromatography in an external buffer (100 mM HEPES, 150 mM NaCl, and 5 mM EDTA at pH 7.4) The lipid concentration was determined by quantitative phosphorus analysis (Bartlett 1959). The vesicles were stored at 4°C.

The calcein fluorescence intensity was monitored at room temperature at an emission wavelength of 515 nm after excitation at 495 nm. Fifty microliters of vesicles with a lipid concentration of 1.69 mM were added to 4 ml of external buffer in a quartz cuvette of 1 cm. After 50 s, an appropriate amount of gp144 was added to obtain the different lipid-to-gp144 molar ratios of 200:1, 100:1, 50:1, and 25:1. After 400 s, 10 μl of a 10% Triton X-100 solution was added to obtain 100% calcein release, and the experiments were stopped after 500 s.

NMR spectroscopy

For NMR experiments, the lipid vesicles were prepared by mixing 20 mg of phospholipids in 180 μl of Tris buffer (50 mM Tris–HCl, pH 7.4) to obtain a solution of 10% (w/w) lipids in buffer. The ^{2}H NMR analyses were performed using an equimolar proportion of deuterated lipids. For the

DMPC:DMPG system, the lipids were codissolved in chloroform. The solvent was removed, and the Tris buffer was subsequently added. Five freeze (liquid nitrogen)/thaw (37°C)/vortex cycles were performed before the addition of 8 mg of gp144, to obtain a lipid-to-gp144 molar ratio of 100:1. The sample was vortexed and used the same day to avoid decrease in protein activity.

^{31}P and ^{2}H solid-state NMR experiments were performed on a Bruker Avance 300 spectrometer (Bruker Biospin, Milton, ON, Canada) operating at frequencies of 121.5 MHz for ^{31}P and 46.1 MHz for ^{2}H. A Hahn echo sequence (Hahn 1950) with TPPM proton decoupling (Bennett et al. 1995) was used for the acquisition of ^{31}P NMR spectra. The ^{31}P NMR spectra were acquired with a 90° pulse length typically of 4 μs, 2,048 complex points, an interpulse delay of 60 μs, and a recycle delay of 4 s. For each temperature, 3,200 scans were collected, and a line broadening of 50 Hz was applied to all spectra. For static ^{31}P experiment, the sample was placed into a 4-mm NMR tube inserted in a home-built probehead. For MAS analysis, a magic-angle spinning probehead (Bruker Biospin) was used. The ^{2}H NMR spectra were acquired with a quadrupolar echo sequence (Davis et al. 1976) using a 90° pulse length typically of 3 μs, an interpulse delay of 60 μs, 4K data points, and a recycle time of 500 ms. For each spectrum, 3,200 scans were collected, and a line broadening of 100 Hz was applied to all spectra. A 1,800-s equilibration delay was allowed between each temperature for all ^{31}P and ^{2}H experiments.

FTIR experiments

CH_2/CD_2 stretching vibrations

Infrared samples were prepared in the same way as for the NMR experiments. The spectra were recorded with a Nicolet Magna 550 Fourier transform spectrometer (Thermo-Nicolet, Madison, WI, USA) equipped with a narrow band mercury–cadmium–telluride (MCT) detector and a germanium-coated KBr beam splitter. The sample (12 μl) was placed between CaF_2 windows separated by a 6-μm Mylar spacer. A total of 100 interferograms were acquired with a resolution of 2 cm^{-1} in the spectral range of 4,000–650 cm^{-1} at various temperatures ranging from 5 to 70°C and controlled by a home-made device. The spectra were corrected for the water-vapor contribution by subtraction of a reference spectrum. The data were processed with the Grams 386 software (Galactic Industries, Salem, MA, USA). The spectral region corresponding to the CH_2 stretching vibrations was baseline-corrected using a cubic function. The methylene symmetric stretching vibration frequency was obtained from the center of gravity calculated at the top 10% of the band.

C=O stretching and amide vibrations

The FTIR spectra in the C=O stretching and amide 1 regions were recorded with a Nicolet Magna 850 Fourier transform spectrometer (Thermo-Nicolet) equipped with a narrow band MCT detector and a germanium-coated KBr beam splitter. A Golden Gate accessory (Specac, Orpington, Kent, UK) was used to record attenuated total reflectance (ATR) spectra at one reflection with a diamond crystal. A total of 100 interferograms were acquired with a resolution of 2 cm^{-1} in the spectral range of 4,000–650 cm^{-1} at 20°C. A uniform sample thickness was ensured by placing a cover for volatile solvents on the sample. The spectra were corrected for the water contribution by subtraction of a reference spectrum (Tris–HCl buffer at pH 7.4). The data were processed with the Grams AI 8 software (Galactic Industries) version 8.0. The spectral region corresponding to the ester carbonyl and amide I regions was baseline-corrected using a cubic function, as proposed by Griffiths and Pariente (1986). The ester carbonyl and amide I regions were also deconvolved using a narrowing factor of 1.6 and an apodization factor of 50%. The different spectral contributions in the amide I region were revealed using the second derivation method (Savitzky and Golay 1964).

Circular dichroism

Small unilamellar vesicles (SUV) were prepared by dispersing 5 mg of lipids into 250 μl of Tris buffer. The lipids were first dissolved in chloroform for the DMPC:DMPG samples. The solvent was removed, and the Tris buffer was subsequently added. After five freeze/thaw cycles, the lipid solutions were extruded 11 times using a 0.1-μm polycarbonate filter according to the Avanti Mini-Extruder procedures (Avanti Polar Lipids, Alabaster, AL, USA). CD spectra were measured with a Jasco J-710 spectropolarimeter (Jasco, Easton, MD, USA). All measurements were made at 20°C in a quartz cuvette of 0.2-mm path length. A 50-μl aliquot of each unilamellar lipid vesicle preparation was combined with 166 μM of purified gp144 to obtain a lipid-to-gp144 ratio of 100:1.

Langmuir isotherms and Brewster angle microscopy

Solutions of DMPC, DMPC, and DMPC:DMPG were prepared at a fixed concentration of 1 mg/ml in chloroform while a solution of gp144 was prepared at 1 mg/ml in Tris buffer. Distilled water purified with a Millipore Milli-Q filtering system with a resistivity of 18.2 MΩcm was used to make the protein solution and the subphase. The experimental setup consisted of a commercial computerized Langmuir trough (Nima Technology, Coventry,

England) onto which was mounted a BAM 2 plus Brewster angle microscope manufactured by Nanofilm Technology (Göttingen, Germany). Surface pressures were measured using a filter paper Wilhelmy plate.

For all experiments, 45 µl of lipids was spread onto a 200 mM NaCl subphase. After a 30-min incubation time to allow chloroform evaporation, gp144 was added underneath the subphase to obtain a lipid-to-protein molar ratio of 100:1. The isotherms were first monitored, and images of the monolayers were recorded at specific surface pressures (10 and 20 mN/m). Prior to imaging the monolayers, the incident 532-nm wavelength Nd:YAG laser and the CCD camera were set at the Brewster angle. The BAM image size was 220 × 275 µm, and the lateral resolution was 1 µm. The geometrical corrections were performed with the Nanofilm Technology software provided with the microscope.

Results and discussion

Gp144 structure

Gp144 contains a weakly positively charged region in the N-terminal domain, as shown in blue in Fig. 1, followed by a hydrophobic α-helical region. The solvent-accessible surface representation with electrostatic potential shown in red is negatively charged in the canyon-like structure of the active site. The physical parameters for these calculations are presented in Table 1 and the calculated gp144 solvation energy was −3,624.3 kcal/mol.

Interaction between gp144 and lipid bilayers

Fluorescence spectroscopy

Fluorescence spectroscopy was used to determine the ability of the gp144 protein to destabilize lipid bilayers. This technique has been extensively used to study the effects of antimicrobial peptides on lipid membranes (Polozov et al. 1994; Sitaram and Nagaraj 1993). Assays with calcein-containing vesicles previously demonstrated that gp144 permeabilized anionic vesicles (DMPG) but had no effect on the stability of zwitterionic membranes (DMPC) (Paradis-Bleau et al. 2007). More specifically, fluorescence spectroscopy was used in the present study to investigate the effect of gp144 on vesicle permeability at different lipid-to-protein molar ratios. The experiments were performed using POPG in the fluid phase at room temperature ($T_m = -2°C$).

Figure 2 shows the calcein release induced by gp144 as a function of time over a period of 500 s. For the 25:1 POPG-to-gp144 ratio, 40% of the calcein was released after 400 s. The remaining calcein released after 400 s was plotted for each of the POPG-to-gp144 ratios (Fig. 3). There is an exponential relationship between the POPG-to-gp144 molar

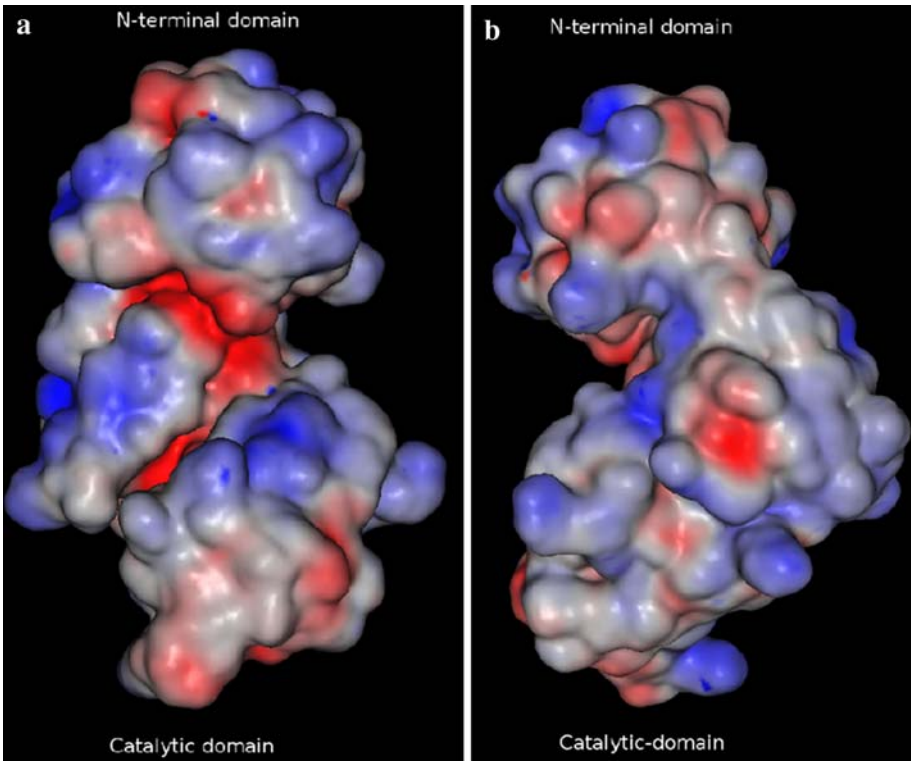

Fig. 1a, b Molecular graphics views of the bacteriophage ϕKZ transglycosylase gp144 (PDB:3BKH). **a** The solvent-accessible surfaces with positive and negative electrostatic potentials are represented in *blue* and *red*, respectively. **b** The gp144 protein has been rotated by 180°

Table 1 PBEQ physical parameters (Sunhwan et al. 2008) for gp144

Parameter	Value	Description
epsR	1.0	Dielectric constant for the reference environment
epsP	1.0	Dielectric constant for the protein interior
epsW	80.0	Solvent dielectric constant
Conc	0.15	Salt concentration (moles/l)
Focus	Yes	To have a refined calculation focused on the site using a finer grid
Dcel_c	1.50	Grid spacing in the finite-difference (centered on Xcen, Ycen, Zcen)
Dcel_f	1.0	Grid spacing in the finite-difference (centered on Xcen, Ycen, Zcen)
LEdge	10.0	Distance between a protein atom and a grid

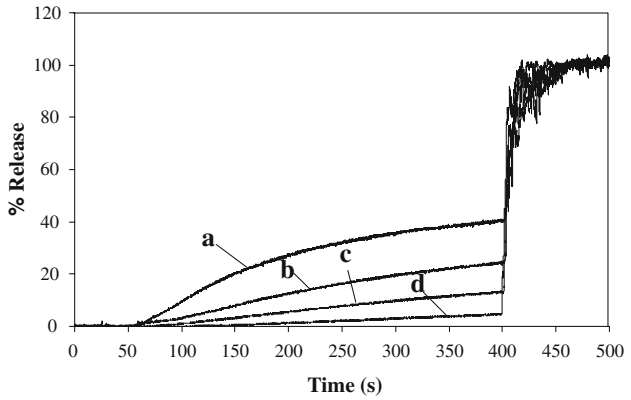

Fig. 2 Calcein release induced by the addition of gp144 to POPG vesicles at different lipid-to-protein molar ratios. **a** 25:1, **b** 50:1, **c** 100:1, and **d** 200:1

ratio and the calcein leakage after 400 s, indicating that gp144 is more efficient at permeabilizing DMPG vesicles at lower POPG-to-gp144 ratios. Based on these results, a 100:1 POPG-to-gp144 ratio was chosen for all other experiments. The gp144 activity was not affected by the lipid phase transition temperature since the results obtained with POPG were similar to those obtained with DMPG.

^{31}P static and MAS NMR

The effect of gp144 on lipid membranes has been investigated by ^{31}P solid-state NMR. ^{31}P NMR is particularly useful for obtaining information about the lipid phase and the orientation and/or dynamic of the polar head group (Seelig 1978; Smith and Ekiel 1984; Watts et al. 1995).

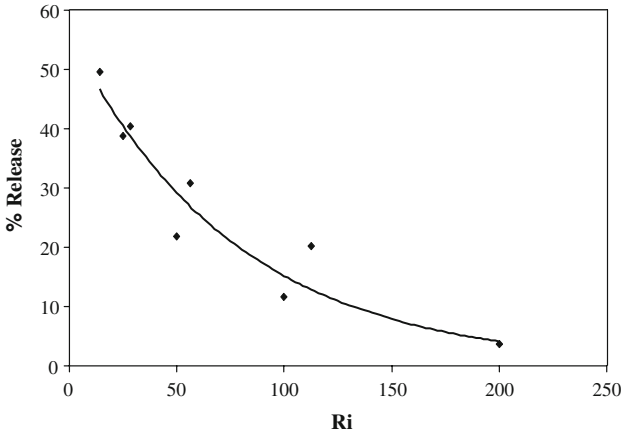

Fig. 3 Percentage of calcein release induced by the addition of gp144 to POPG vesicles as a function of the lipid-to-protein molar ratio (Ri) after 400 s

Indeed, the spectrum is dominated by the chemical shift anisotropy (CSA), and the shape of the spectrum is related to a specific lipid phase. The ^{31}P nucleus is located in the lipid polar head group and can be used without labeling (100% natural abundance).

Figure 4 shows the effect of gp144 on three different lipid systems. The ^{31}P NMR spectra of the pure lipid systems are characteristic of lipids in a lamellar phase. The spectrum obtained for DMPC in the presence of gp144 is also characteristic of lipids in a lamellar phase. The data obtained are in agreement with previous fluorescence results showing absence of gp144-induced lysis for the DMPC vesicles (Paradis-Bleau et al. 2007). However, we noticed a small broadening of the spectrum, which can be associated with an interaction of gp144 with neutral lipids. For the DMPG and DMPC:DMPG systems, the spectra presented in Fig. 4 show isotropic signals that could be due to the formation of small isotropic structures or of a cubic phase (Ekiksson and Lindblom 1987) co-existing with a lamellar phase. The preferential or specific interactions between antimicrobial peptides or proteins have been observed with anionic lipids (Bechinger 2004; Hori et al. 1999; Ramamoorthy 2009). In addition, the presence of isotropic phases is characteristic of the interaction between toxic proteins or antimicrobial peptides and lipid bilayers (Bechinger 2005; Chia et al. 2000; Picard et al. 1996; Ramamoorthy 2009). For example, Batenburg et al. (1985) showed that cardiolipin induces an isotropic phase in POPG:POPC mixtures. In addition, the detergent-like properties of magainin antibiotic peptides have been demonstrated by ^{31}P NMR spectroscopy (Bechinger 2005). On the other hand, the formation of cubic phases has been observed in zwitterionic membranes in the presence of the peptide pardaxin (Hallock et al. 2002). It is not possible however with the results obtained in the present study to

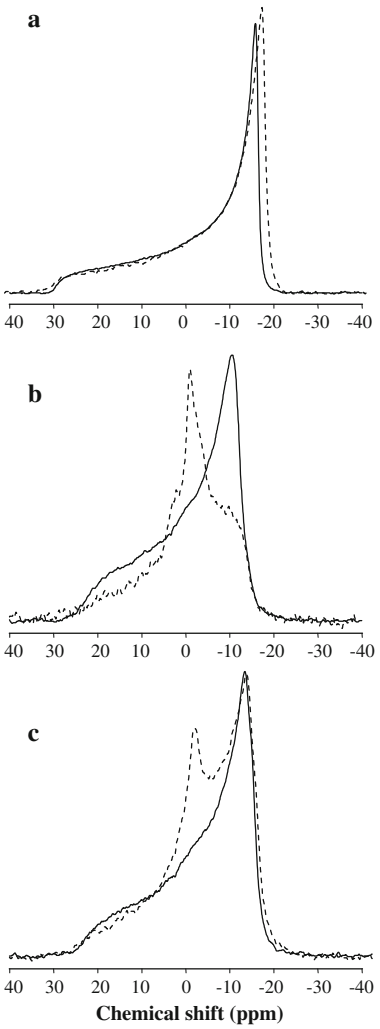

Fig. 4a–c ^{31}P static NMR spectra of the different lipid systems in the absence (*solid*) and presence (*dotted*) of gp144 at a lipid-to-protein molar ratio of 100:1 at 37°C. **a** DMPC, **b** DMPG, and **c** DMPC:DMPG 1:1

differentiate between the formation of small vesicles or cubic structures in the presence of gp144.

The coexistence of lamellar and isotropic phases revealed two distinct populations of lipids, one affected by the presence of gp144 and forming small or cubic structures, while the other group of lipids was not affected and remained in a lamellar phase. The proportion of lipids in isotropic structures has been calculated, and the results are presented in Table 2. For the pure DMPG system, 45% of the lipids were in an isotropic phase, whereas 27% was obtained for the DMPC:DMPG system. This indicated that the proportion of anionic lipids influenced the interaction of gp144 with model membranes. This also suggested that an increase in the proportion of anionic lipids promotes the interaction between gp144 and model membranes.

We have also investigated the effect of gp144 on the orientation and/or dynamic of the lipid head groups present

Table 2 ^{31}P NMR parameters obtained for the lipid systems in the presence of gp144

System	% Isotropic phase	S_2
DMPC	0	1.07 ± 0.03
DMPG	45 ± 5	0.9 ± 0.1
DMPC:DMPG	27 ± 5	0.9 ± 0.1

in the lamellar phases. The comparison of the chemical shift anisotropies obtained in the absence or presence of the protein was done via the calculation of an order parameter S_2 proposed by Picard et al. (1999):

$$S_2 = \frac{\delta}{\delta_{\text{ref}}} \quad (1)$$

where δ is the CSA measured for a lipid system in the presence of gp144 and δ_{ref} is the CSA of the pure lipid system. S_2, related to the second spectral moment, is equal to 1 for a system in which the orientation and/or dynamics of the lipid head groups are the same with or without gp144 and is equal to 0 if the system becomes totally isotropic (Picard et al. 1999). The value of the S_2 parameter of 1.07 for the DMPC:gp144 system indicated that the interaction of the protein with zwitterionic lipids resulted in a slight change in orientation or a rigidification of the DMPC head group. For the DMPG:gp144 and DMPC:DMPG:gp144 systems, the small decrease in the S_2 parameters to a value of 0.9 indicated a small change in orientation or an increase in the dynamic of the lamellar phase lipids. However, the shape of the powder spectra did not differ significantly in the presence of gp144, indicating that the presence of the protein does not induce any significant change in the orientation of the multilamellar vesicles in the magnetic field.

The three systems were also studied by high-resolution ^{31}P MAS NMR. The use of magic-angle spinning allows the averaging of the CSA and therefore the investigation of the effect of the protein on each component of the MLV (Pinheiro and Watts 1994). The MAS spectra presented in Fig. 5 depict two isotropic resonances. The high-frequency resonance was assigned to DMPG and the low-frequency resonance to DMPC. Figure 5a demonstrates that the presence of gp144 had no significant effect on zwitterionic lipids except for a slight narrowing of the spectra. This narrowing was also observed for the DMPC resonance in the DMPC:DMPG:gp144 system and could be due to a stabilization of the membrane by gp144 (Smith and Ekiel 1984). This is consistent with the increase in the CSA observed in the static ^{31}P NMR spectrum of the DMPC:gp144 system. The presence of gp144 in anionic lipids induced a significant upfield shift of the resonances (Fig. 5b, c), reflecting changes in the membrane charge density (Bonev et al. 2001). This result is typical of

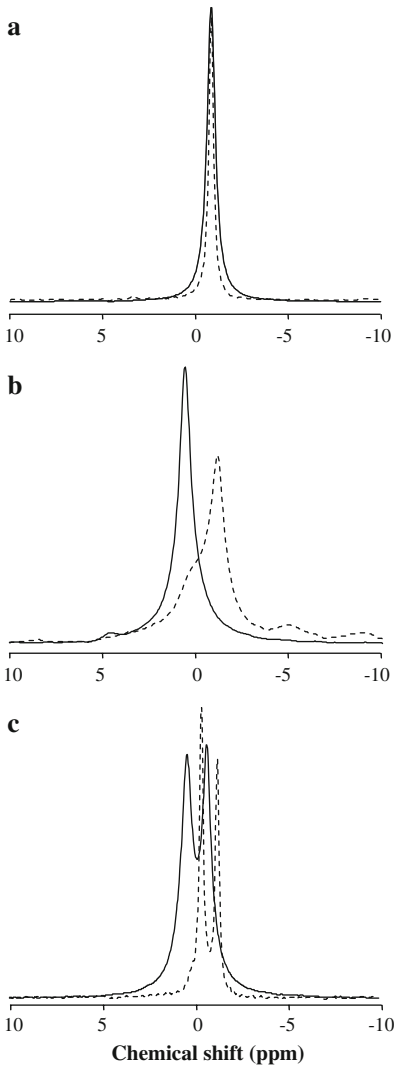

Fig. 5a–c ^{31}P MAS NMR spectra of the different lipid systems in the absence (*solid*) and presence (*dotted*) of gp144 at a lipid-to-protein molar ratio of 100:1 at 37°C. **a** DMPC, **b** DMPG, and **c** DMPC:DMPG 1:1

electrostatic interactions between the protein and the lipid head group. A similar effect has been observed in the interaction of the antibiotic peptide LaH4 and anionic lipid membranes (Mason et al. 2006). It is interesting to note that in the DMPC:DMPG:gp144 system, both lipids are affected by gp144. A similar effect was observed in the interaction of the antimicrobial peptide cupiennin 1a with DMPC/DMPG MLV (Pukala et al. 2007) and by Carbone and Macdonald (1996) for POPG:POPC MLV in interaction with cardiotoxin. In this latter case, however, the addition of cardiotoxin first influenced POPG, and a higher concentration of the protein was required to influence the POPC resonance (Carbone and Macdonald 1996). In our case, a lipid-to-protein molar ratio of 100:1 was sufficient to influence both the DMPC and DMPG resonances in the system. The results presented in Fig. 5 also indicated that only a portion of the lipids of the pure DMPG system were influenced by the protein, while all lipids appeared to be affected for the DMPC:DMPG:gp144 system.

Deuterium NMR

We have also investigated the effect of gp144 on the hydrophobic region of DMPC and DMPC:DMPG bilayers by ^{2}H NMR spectroscopy. This was achieved using phospholipids with deuterated acyl chains (DMPC-d_{54}). The deuteration of the lipid acyl chains does not significantly alter the properties of the synthetic membrane organization except for the main phase transition temperature, which is decreased by 3–5°C (Guard-Friar et al. 1985). It is thus possible to determine variations in the lipid chain order by monitoring changes in the quadrupolar splitting ($\Delta\nu_Q$) values. The increase or decrease in $\Delta\nu_Q$ for a C–D bond in a lipid bilayer system with axial symmetry is associated with ordering or disordering of the deuterated chains, respectively, and is related to the order parameter S_{CD}:

$$\Delta\nu_Q = \frac{3e^2qQ}{4\ \ h}\left(3\cos^2\theta - 1\right)S_{CD} \qquad (2)$$

where (e^2qQ/h) is the quadrupole coupling constant for C–D bonds ($\sim$167 kHz) and θ is the angle between the bilayer normal and B_0 (Seelig and Seelig 1980).

The presence of gp144 at a lipid-to-protein molar ratio of 100:1 did not significantly affect the order of the DMPC acyl chains (Fig. 6a). A similar result was obtained for the DMPC:DMPG:gp144 system (Fig. 6b). However, the spectrum presented in Fig. 6b shows a significant isotropic contribution, confirming the presence of two populations of lipids in the mixed system, one influenced by the presence of gp144 (isotropic contribution) and one that was not influenced by the protein (no change in the quadrupolar splitting). This result also indicated that gp144 interacts with the zwitterionic lipids when they are mixed with anionic lipids and also confirmed that there is formation of isotropic structures only in the presence of anionic lipids.

FTIR spectroscopy, lipid acyl chains

We have used FTIR spectroscopy to complement the ^{2}H NMR study measuring the effect of gp144 on lipid acyl chains. This technique has been shown to be very useful for investigating lipid–protein interactions from the study of the lipid CH_2, CD_2, and C=O stretching vibrations (Mantsch and McElhaney 1991). The study of the CH_2 symmetric (2,850 cm^{-1}) and CD_2 antisymmetric (2,195 cm^{-1}) stretching vibrations, which are sensitive to *trans/gauche* isomerization in the lipid acyl chains, can provide valuable information about the order of the acyl chains and the lipid

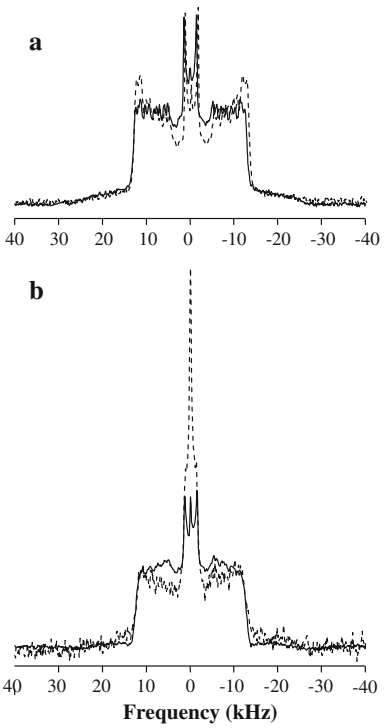

Fig. 6a, b ^{2}H NMR spectra of the different lipid systems in the absence (*solid*) and presence (*dotted*) of gp144 at a lipid-to-protein molar ratio of 100:1 at 37°C. **a** DMPC-d_{54} and **b** DMPC-d_{54}:DMPG 1:1

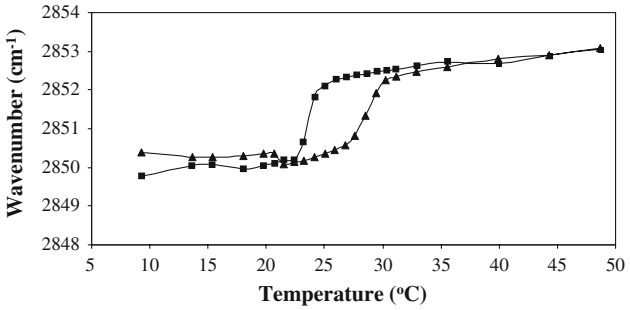

Fig. 7 Temperature dependence of the CH_2 symmetric stretching vibration of pure DMPG (*square*) and DMPG:gp144 (*triangle*) at a lipid-to-protein molar ratio of 100:1

Table 3 Variation of the lipid phase transition temperature in the presence of gp144

System	ΔT (°C)
DMPC:gp144	2 ± 1
DMPG:gp144	7 ± 2
DMPC:DMPG:gp144	DMPC: 6 ± 2
	DMPG: 7 ± 2

phase transition temperature (Mantsch and McElhaney 1991).

The frequencies of the CH_2 stretching vibration as a function of temperature obtained for the DMPG system in the absence and presence of gp144 are shown in Fig. 7. These results indicated a large increase in the lipid phase transition temperature (by 7°C) upon the addition of gp144 at a 100:1 lipid-to-protein molar ratio. An increase in the lipid phase transition temperature is generally observed in the case of electrostatic interactions (Richard et al. 2002). The results presented in Table 3 indicate a small increase (by 2°C) in the DMPC phase transition temperature in the presence of gp144. This is in agreement with the results obtained by ^{31}P NMR, suggesting a stabilization of the zwitterionic membranes in the presence of gp144. Analysis of the frequencies of the CD_2 antisymmetric (DMPC-d_{54}) and CH_2 symmetric (DMPG) vibrations in the mixed system indicated a significant increase in the phase transition temperature for both lipids (by 6°C for DMPC and 7°C for DMPG). This result confirmed that gp144 interacts with zwitterionic lipids when mixed with anionic lipids, with a similar effect of gp144 on DMPC and DMPG. It also confirmed the ^{31}P MAS NMR study in which the effect on both lipids was almost the same in the mixed lipid sample.

FTIR spectroscopy, interfacial region

Analysis of the carbonyl stretching vibrations in FTIR spectra can provide information about the effect of proteins on the lipid interfacial region. The C=O stretching vibration, centered at 1,733 cm^{-1}, is the superposition of two bands, one centered at 1,740 cm^{-1} and the second at 1,727 cm^{-1} (Lewis et al. 1994). Deconvolution of the broad band allows access to the two contributions (Griffiths and Pariente 1986). These two contributions correspond, respectively, to free and hydrogen-bonded carbonyl groups (Blume et al. 1988). The C=O stretching vibration is sensitive to the gel-to-fluid phase transition and to the hydration of the lipid interfacial region (Lewis et al. 1994).

Figure 8 shows the deconvolved FTIR spectra obtained in the C=O stretching region for DMPC and DMPG systems in the absence and presence of gp144. Both spectra indicated a decrease in the intensity of the 1,727 cm^{-1} contribution in the presence of gp144, which can be associated with a decrease in the water accessibility that could be caused by the presence of the protein in the interfacial region. This result also indicated an interaction between the zwitterionic lipids and gp144. The results presented in Fig. 8b also indicate a significant broadening of the C=O stretching vibrations for DMPG in the presence of gp144, suggesting an increased mobility of the lipid interfacial region. This could presumably be associated with the presence of a significant proportion of isotropic structures in this system. A similar effect was also observed by

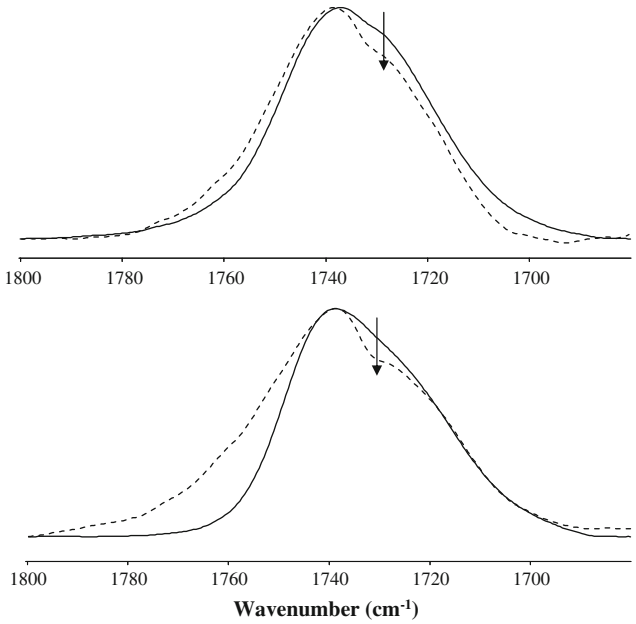

Fig. 8 Deconvolved FTIR spectra in the C=O stretching region of DMPC (*top*) and DMPG (*bottom*) vesicles in the absence (*solid*) and presence (*dotted*) of gp144 at a lipid-to-protein molar ratio of 100:1

Arrondo and Goni (1998) for glycoporin on DPPC membranes. Zhang et al. (1997) reported that the broadening of the ester carbonyl vibration could be associated with an increase in lipid motion in the presence of proteins.

Langmuir films

The study of lipid–protein interactions at the air/water interface is an interesting way to obtain more information about the nature of the interaction (Maget-Dana 1999). Planar lipid systems such as monolayers mimic the lateral organization of phospholipids in cellular membranes (Brockman 1999). The interactions between several peptides and proteins with lipid monolayers have been investigated (Tapanendu et al. 2007; Vitovic et al. 2004). As an amphiphilic molecule, the lipid polar head groups are oriented in the subphase. The monolayer technique can therefore be used to confirm the initial interaction of a protein with the lipid head group.

We have first recorded the surface pressure/area isotherm of gp144 alone to optimize the amount of NaCl needed to avoid the solubilization of gp144 in the subphase. The lowest NaCl concentration yielding a surface pressure/area isotherm of gp144 was 200 mM. The addition of gp144 to DMPC monolayers did not induce any increase in molecular area (data not shown). However, an increase in the molecular area for the DMPG and DMPC:DMPG systems was observed with gp144. The increase in the molecular area for the DMPG monolayer in the presence of gp144 was 3 ± 2 Å/molecule at surface pressures of 10 and 20 mN/m. For the DMPC:DMPG system, the increases in the molecular area were 7 ± 2 and 3 ± 2 Å/molecule at surface pressures of 10 and 20 mN/m, respectively. This increase can be explained by the fact that anionic lipids promote the adsorption of the protein into the monolayer. This result confirmed that the membrane interaction of gp144 is very different for anionic and zwitterionic lipids. More specifically, it suggested that specific electrostatic interactions allow gp144 to penetrate the monolayer of anionic lipids. It is interesting to note that an increase in molecular area in the presence of anionic lipids has already been reported for antimicrobial peptides such as melittin (Hendrickson et al. 1983), cardiotoxin (Bougis et al. 1981), maculatin (Ambroggio et al. 2004), and citropin (Ambroggio et al. 2004). However, the presence of gp144 had no effect on the monolayer collapse pressure.

Brewster angle microscopy

Lipid domains have been shown to be involved in the interaction between proteins and lipid membranes (Brockman 1999; Gil et al. 1998). To visualize these interactions, several techniques such as atomic force microscopy (AFM), two-dimensional photon fluorescence spectroscopy, and Monte-Carlo simulations can be used. In the present study, we have used BAM, a valuable technique to visualize domain formation at different surface pressures at the air–water interface (Volinsky et al. 2006). This in situ technique uses polarized light on a refractive surface such as water. At a specific angle θ, called the Brewster angle and defined by:

$$\tan\theta = n_1/n_2 \quad (3)$$

where n_1 and n_2, respectively, are the refractive indices of air and water, there is no reflected light (Henon and Meunier 1991). BAM associated with Langmuir films allows the visualization of the film organization and domain formation (Volinsky et al. 2004). The experiments were performed by injecting gp144 under compression and beneath the lipid monolayer at specific surface pressures (10 and 20 mN/m) to determine if the protein induces domain formation in monolayers (Volinsky et al. 2006). Significant changes in the molecular area of the DMPG and DMPC:DMPG systems were observed at these surface pressures in the surface pressure/area isotherm results.

Figure 9 shows the BAM results for the DMPC and DMPG systems in the absence and presence of gp144 at two surface pressures. The addition of gp144 at a lipid-to-protein molar ratio of 100:1 did not induce domain formation in DMPC monolayers. However, we noted a small increase in the gray level at the two surface pressures. This increase can be caused by the interaction of gp144 with the

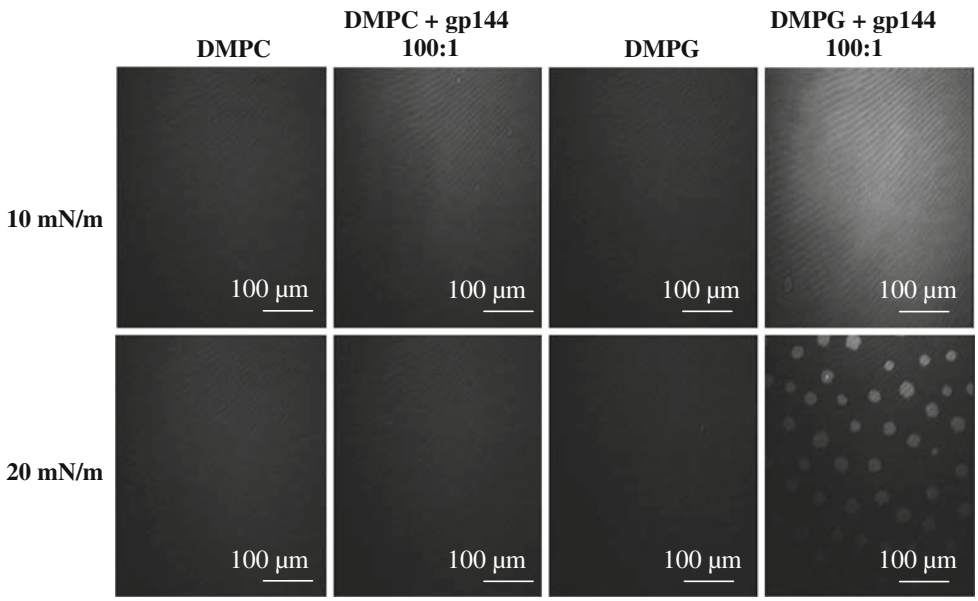

Fig. 9 BAM images of DMPC and DMPG at surface pressures of 10 and 20 mN/m in the absence and presence of gp144 at a lipid-to-protein molar ratio of 100:1

lipid polar head group, the accumulation of gp144 under the monolayer changing the refractive index of the monolayer and inducing a change in the gray level (Winsel et al. 2003). This interaction was not noticeable in the surface pressure/area isotherms, presumably because gp144 does not intercalate into the monolayer. This is in agreement with the ^{31}P NMR results indicating a slight rigidification of the lipid head group upon interaction with the protein.

The effect of gp144 on the DMPG system is different at the two surface pressures; an increase in gray level was observed at 10 mN/m, while lipid domains appeared at 20 mN/m. The size of the domains was about 25 ± 5 µm, and the domains were about 100 µm away from each other. The distance between the domain decreased with increasing surface pressure while the size of each individual domain remained constant (data not shown). We concluded that the formation of domains is possible at physiological surface pressure, the surface pressure of a natural lipid bilayer being about 30 mN/m. It is well know that interactions between a protein and a lipid monolayer are promoted at higher surface pressures (Demel et al. 1975) when the concentration of anionic charges is increased. Therefore, the behavior of monolayers at higher surface pressures can be extrapolated to bilayers (Marsh 1996).

A similar behavior was observed for the DMPC:DMPG:gp144 system, namely an increase in the gray level at 10 mN/m and the same shape of domains at 20 mN/m (data not shown). Lipid domains in biological membranes are known to be the key to the initial recognition of proteins for different biological phenomena (Brown and London 2000). However, a recent study demonstrated that the interactions between an antimicrobial peptide and a lipid monolayer promote the aggregation of the peptide (Volinsky et al. 2004, 2006). In the present study, the observed domains do not have the characteristic shape of aggregated peptides. However, their shape is more similar to the one observed for mixed lipid domains (Arnold et al. 2005). These results suggest that the gp144 protein has a different mode of action than small antimicrobial peptides.

Protein structural change

Circular dichroism

To confirm the importance of the lipid charge for membrane interaction of gp144 and to investigate potential changes in the gp144 secondary structure upon lipid binding, we have performed circular dichroism experiments (Berova et al. 2000; Elliott and Ambrose 1950) as a function of DMPG proportion in unilamellar lipid vesicles. The crystal structure of gp144 reveals that the protein mainly adopts an α-helical conformation (Fokine et al. 2008). A previous study showed a decrease in the molar ellipticity of gp144 at 222 nm upon binding to anionic lipids, suggesting a decrease in the α-helical structure content of gp144 (Paradis-Bleau et al. 2007). However, this study did not observe a change in protein secondary structure upon binding to zwitterionic lipids. Results obtained in the present study indicated that the molar ellipticity at 222 nm decreased when the proportion of anionic lipids increased in unilamellar lipid vesicles (Fig. 10). This confirmed the importance of the lipid negative charge in the interaction between gp144 and model membranes. However, the decrease in ellipticity could be induced by light scattering due to a change in the vesicle structure (Jelokhani-Niaraki et al. 2002), as suggested by

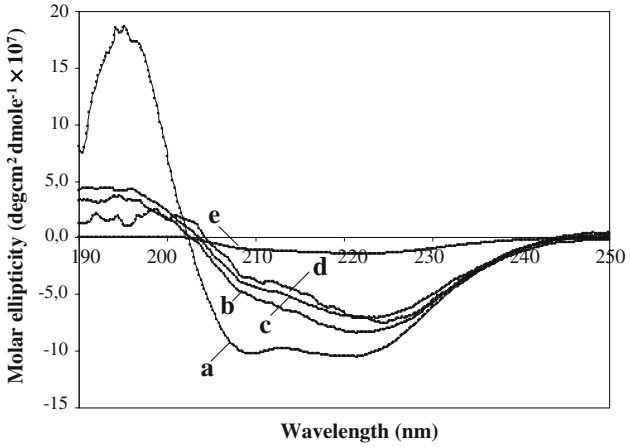

Fig. 10a–e CD spectra of gp144 in interaction with DMPC:DMPG vesicles at different DMPG ratios. **a** 0% PG, **b** 25% PG, **c** 50% PG, **d** 75% PG, and **e** 100% PG

the ^{31}P NMR results and the change in the visual appearance of the sample upon protein binding.

FTIR, protein structure

Fourier transform infrared spectroscopy was used to discriminate between gp144 structural change and light scattering. The amide I and II vibrations of FTIR spectra provide useful information for the study of protein secondary structures (Goormaghtigh et al. 1994). The amide I vibration is due primarily to C=O stretching, while the amide II vibration comes from NH bending (Kong and Yu 2007). As the amide I band is masked by the water signal, it is necessary to either perform the experiment in D_2O or to subtract the water signal. In our case, the use of D_2O was not possible since it altered the enzymatic activity of gp144. Indeed, the increase in the lipid phase transition temperature seen by FTIR spectroscopy was completely abolished when the samples were prepared in D_2O (data not shown). The protein structure was not changed however in D_2O, as determined from the analysis of the amide I band (results not shown). The water signal was then subtracted by the method described by Dousseau et al. (1989), and the ATR technique was used with a Golden Gate single reflection diamond sample holder to allow the acquisition of low absorption spectra with good signal-to-noise ratios.

The spectral components of the amide I and II bands were obtained using the second derivative method described by Savitzky and Golay (1964). The major signal at 1,655 cm^{-1} in the amide I region confirmed that gp144 adopts an α-helical conformation (Fig. 11a, solid line). This result was confirmed by the presence of a band at 1,545 cm^{-1} in the amide II region (Barth 2007). In addition to the α-helix signal, the FTIR spectrum of gp144 in both the amide I and amide II regions showed contributions that can be associated with intermolecular antiparallel β-sheets (Barth 2007). The combination of bands at 1,690 and 1,620 cm^{-1} indicated a partial aggregation of gp144 in solution (Arrondo et al. 1988).

The α-helical conformation of gp144 was maintained in the presence of model membranes (Fig. 11, dotted line), but there was a decrease in protein aggregation in the DMPC and DMPG lipid systems. These results confirm the interaction between gp144 and the zwitterionic lipid DMPC, even in the absence of vesicle lysis. However, the decrease in gp144 aggregation was more important in the DMPG system. Indeed, the intensity of the amide I band components at 1,690 and 1,620 cm^{-1} and of the amide II

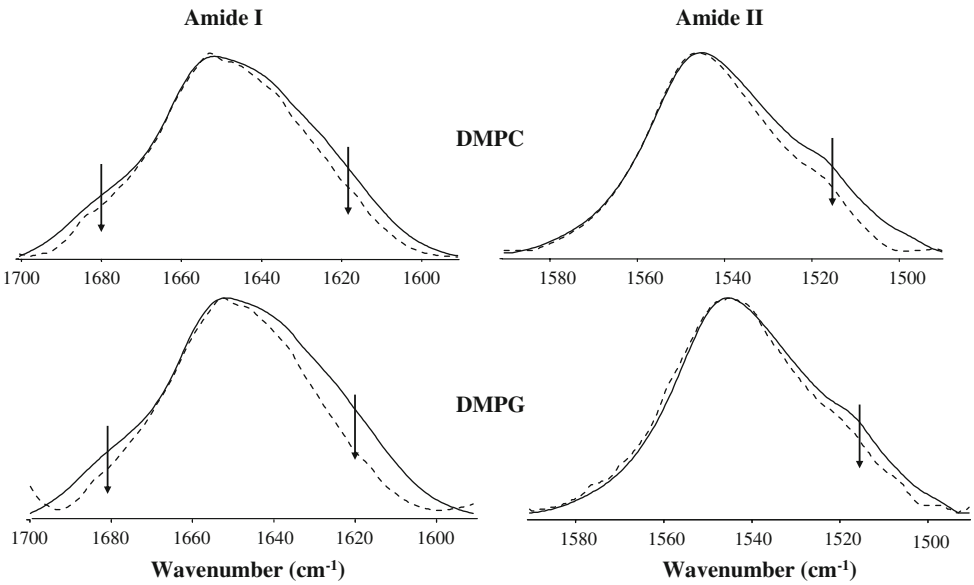

Fig. 11 Deconvolved FTIR spectra in the amide I and amide II regions of gp144 in the absence (*solid*) and presence (*dotted*) of DMPC and DMPG at a lipid-to-protein molar ratio of 100:1

band component at 1,516 cm^{-1} decreased more in the anionic lipid model than in the zwitterionic lipid model. This suggested that electrostatic interactions between gp144 and anionic membranes are promoted before the aggregation of the protein. It also confirmed the BAM results, indicating the absence of protein aggregation in monolayers. We can therefore conclude that the decrease in molar ellipticity at 222 nm observed in circular dichroism spectra is the result of light scattering and does not reflect significant change in gp144 secondary structure.

Conclusions

The aim of our study was to understand how gp144 disorganizes bacterial membranes to access the targeted periplasmic peptidoglycan. The different techniques used in the present study confirmed the preferential electrostatic interactions between gp144 and anionic model membranes (DMPG). More specifically, the membrane permeabilizing properties of gp144 in anionic membranes were demonstrated by fluorescence spectroscopy, while the formation of isotropic structures was evidenced by ^{31}P NMR spectroscopy. In addition, deuterium NMR indicated that gp144 has no significant effect on the order of the DMPC acyl chains, suggesting an interaction at the level of the charged lipid polar head group. A significant increase in the anionic lipid phase transition temperature upon protein binding was evidenced by FTIR spectroscopy, again suggesting strong electrostatic interactions. BAM revealed the formation of lipid domains at surface pressures close to that of lipid bilayers (Marsh 1996). Finally, FTIR spectroscopy indicated that there is no major change in the protein secondary structure upon interaction with lipid membranes.

Our results therefore suggest that the weakly positively charged region in the N-terminal domain of gp144 would be responsible for the initial electrostatic interactions with the charged lipid polar head groups of the bacterial membrane. This initial interaction would then induce the formation of isotropic lipid structures or lipid domains, enhancing membrane permeabilization. Gp144 would thus be able to access and hydrolyze the periplasmic peptidoglycan. Our results also demonstrated an interaction of gp144 with zwitterionic lipids but confirmed that this interaction does not yield to a disruption of the membrane structure. This suggested that gp144 would presumably have minimal effect on the membranes of eukaryotic cells. In order to confirm the role of the N-terminal region of gp144 for membrane interaction and permeabilization, specific mutations of charged residues will be done and the proteins obtained will be analyzed by the biophysical techniques described in the present study. Further studies could also be performed with a small peptide mimicking the weakly positively charged region in the N-terminal domain of gp144.

Acknowledgments The authors thank Pierre Audet, Patricia Basque, Nathalie Desgagné, François Lapointe, and François Sanschagrin for their technical assistance and helpful discussions. We also thank Halim Maaroufi from the Plateforme de bioinformatique, Institut de Biologie Intégrative et des Systèmes, for his excellent technical assistance in computer-assisted modeling. This work was supported by the Natural Science and Engineering Research Council (NSERC) of Canada, the Fonds Québécois de la Recherche sur la Nature et les Technologies (FQRNT), the Canadian Institutes for Health Research (CIHR), the Canadian Cystic Fibrosis Foundation, the Centre de Recherche sur la Structure, la Fonction et l'Ingénierie des Protéines (CREFSIP), and the Centre de Recherche en Sciences et Ingénierie des Macromolécules (CERSIM). Catherine Paradis-Bleau also thanks the Fonds sur la Recherche en Santé du Québec (FRSQ) for a graduate scholarship.

References

Ackermann HW (2003) Bacteriophage observations and evolution. Res Microbiol 154:245–251

Ambroggio EE, Separovic F, Bowie J, Fidelio GD (2004) Surface behaviour and peptide-lipid interactions of the antibiotic peptides, maculatin and citropin. Biochim Biophys Acta 1664:31–37

Arnold A, Cloutier I, Ritcey AM, Auger M (2005) Temperature and pressure dependent growth and morphology of DMPC/DSPC domains studied by Brewster angle microscopy. Chem Phys Lipids 133:165–179

Arrondo JL, Goni FM (1998) Infrared studies of protein-induced perturbation of lipids in lipoproteins and membranes. Chem Phys Lipids 96:53–68

Arrondo JL, Young NM, Mantsch HH (1988) The solution structure of concanavalin A probed by FT-IR spectroscopy. Biochim Biophys Acta 952:261–268

Barth A (2007) Infrared spectroscopy of proteins. Biochim Biophys Acta 1767:1073–1101

Bartlett GR (1959) Phosphorus assay in column chromatography. J Biol Chem 234:466–468

Batenburg AM, Bougis PE, Rochat H, Verkleij AJ, de Kruijff B (1985) Penetration of a cardiotoxin into cardiolipin model membranes and its implications on lipid organization. Biochemistry 24:7101–7110

Bechinger B (2004) Structure and function of membrane-lytic peptides. Crit Rev Plant Sci 23:271–292

Bechinger B (2005) Detergent-like properties of magainin antibiotic peptides: a ^{31}P solid-state NMR spectroscopy study. Biochim Biophys Acta 1712:101–108

Bennett AE, Rienstra CM, Auger M, Lakshmi KV, Griffin RG (1995) Heteronuclear decoupling in rotating solids. J Chem Phys 103:6951–6958

Berova N, Nakanishi K, Robert WW (2000) Circular dichroism: principles and applications. Wiley, New York, p 877

Blume A, Hubner W, Messner G (1988) Fourier transform infrared spectroscopy of ^{13}C=O-labeled phospholipids hydrogen bonding to carbonyl groups. Biochemistry 27:8239–8249

Bonev B, Watts A, Bokvist M, Grobner G (2001) Electrostatic peptide-lipid interactions of amyloid-β peptide and pentalysine with membrane surfaces monitored by ^{31}P MAS NMR. Phys Chem Chem Phys 3:2904–2910

Borysowski J, Weber-Dabrowska B, Gorski A (2006) Bacteriophage endolysins as a novel class of antibacterial agents. Exp Biol Med 231:366–377

Bougis P, Rochat H, Pieroni G, Verger R (1981) Penetration of phospholipid monolayers by cardiotoxins. Biochemistry 20: 4915–4920

Briers Y, Volckaert G, Cornelissen A, Lagaert S, Michiels CW, Hertveldt K, Lavigne R (2007) Muralytic activity and modular structure of the endolysins of *Pseudomonas aeruginosa* bacteriophages phiKZ and EL. Mol Microbiol 65:1334–1344

Brockman H (1999) Lipid monolayers: why use half membrane to characterize protein-membrane interactions? Curr Opin Struct Biol 9:438–443

Brown DA, London E (2000) Structure and function of sphingolipid- and cholesterol-rich membrane rafts. J Biol Chem 275:17221–17224

Carbone MA, Macdonald PM (1996) Cardiotoxin II segregates phosphatidylglycerol from mixtures with phosphatidylcholine: ^{31}P and ^{2}H NMR spectroscopic evidence. Biochemistry 35:3368–3378

Chia BCS, Lam YH, Dyall-Smith M, Separovic F, Bowie JH (2000) A ^{31}P NMR study of the interaction of amphibian antimicrobial peptides with the membranes of live bacteria. Lett Peptide Sci 7:151–156

Davies JC (2002) *Pseudomonas aeruginosa* in cystic fibrosis: pathogenesis and persistence. Paediatr Respir Rev 3:128–134

Davis JH, Jeffrey KR, Bloom M, Valic MI, Higgs TP (1976) Quadrupolar echo deuteron magnetic resonance spectroscopy in ordered hydrocarbon chains. Chem Phys Lett 42:390–394

Demel RA, Geurts Van Kessel WSM, Zwall RFA, Roelofsen B, Van Deenen LM (1975) Relation between various phospholipase actions on human red cell membranes and the interfacial phospholipid pressure in monolayers. Biochim Biophys Acta 406:97–107

Dousseau F, Therrien M, Pézolet M (1989) On the spectral substraction of water from the FT-IR spectra of aqueous solutions of proteins. Appl Spectrosc 43:538–542

Ekiksson P-O, Lindblom G (1987) NMR studies of micellar aggregates in 1-acyl-sn-glycerophosphocholine systems. The formation of a cubic liquid crystalline phase. J Phys Chem 91:846–853

Elliott A, Ambrose EJ (1950) Structure of synthetic polypeptides. Nature 165:921–922

Fischetti VA (2001) Phage antibacterials make a comeback. Nat Biotechnol 19:734–735

Fischetti VA (2005) Bacteriophage lytic enzymes: novel anti-infectives. Trends Microbiol 13:491–496

Fokine A, Miroshnikov KA, Shneider MM, Mesyanzhinov VV, Rossmann MG (2008) Structure of the bacteriophage phiKZ lytic transglycosylase, gp144. J Biol Chem 283:7242–7250

Gil T, Ipsen JH, Mouritsen OG, Sabra MC, Sperotto MM, Zuckermann MJ (1998) Theoretical analysis of protein organization in lipid membranes. Biochim Biophys Acta 1376:245–266

Goormaghtigh E, Cabiaux V, Ruysschaert J-M (1994) Determination of soluble and membrane protein structure by Fourier transform infrared spectroscopy. I. Assignments and model compounds. Subcell Biochem 23:329–362

Griffiths PR, Pariente GL (1986) Introduction to spectral deconvolution. Trends Anal Chem 5:209–215

Guard-Friar D, Chen C-H, Engle AS (1985) Deuterium isotope effect on the stability of molecules: phospholipids. J Phys Chem J Phys Chem 89:1810–1813

Hahn EL (1950) Spin echoes. Phys Rev 80:580

Hallock KJ, Lee DK, Omnaas J, Mosberg HI, Ramamoorthy A (2002) Membrane composition determines pardaxin's mechanism of lipid bilayer disruption. Biophys J 83:1004–1013

Hendrickson HS, Fan PC, Kaufman DK, Kleiner DE (1983) The effect of a phase transition on penetration of phospholipid monolayers by melittin and glucagon. Arch Biochem Biophys 227:242–247

Henon S, Meunier J (1991) Microscope at the Brewster angle: direct observation of first-order phase transitions in monolayers. Rev Sci Instrum 64:936–939

Hori Y, Demura M, Niidome T, Aoyagi H, Asakura T (1999) Orientational behavior of phospholipid membranes with mastoparan studied by ^{31}P solid state NMR. FEBS Lett 455: 228–232

Jelokhani-Niaraki M, Prenner EJ, Kay CM, McElhaney RN, Hodges RS (2002) Conformation and interaction of the cyclic cationic antimicrobial peptides in lipid bilayers. J Peptide Res 60:23–36

Kong J, Yu S (2007) Fourier transform infrared spectroscopic analysis of protein secondary structures. Acta Biochim Biophys Sin 39:549–559

Lewis RNAH, McElhaney RN, Pohle W, Mantsch HH (1994) Components of the carbonyl stretching band in the infrared spectra of hydrated 1, 2-diacylglycerolipid bilayers: a reevaluation. Biophys J 67:2367–2375

Maget-Dana R (1999) The monolayer technique: a potent tool for studying the interfacial properties of antimicrobial and membrane-lytic peptides and their interactions with lipid membranes. Biochim Biophys Acta 1462:109–140

Mantsch HH, McElhaney RN (1991) Phospholipid phase transitions in model and biological membranes as studied by infrared spectroscopy. Chem Phys Lipids 57:213–226

Marsh D (1996) Lateral pressure in membranes. Biochim Biophys Acta 1286:183–223

Mason AJ, Martinez A, Glaubitz C, Danos O, Kichler A, Bechinger B (2006) The antibiotic and DNA-transfecting peptide LAH4 selectively associates with, and disorders, anionic lipids in mixed membranes. FASEB J 20:320–322

Mesyanzhinov VV, Robben J, Grymonprez B, Kostyuchenko Victor A, Bourkaltseva Maria V, Sykilinda Nina N, Krylov Victor N, Volckaert G (2002) The genome of bacteriophage phiKZ of *Pseudomonas aeruginosa*. J Mol Biol 317:1–19

Morita M, Tanji Y, Orito Y, Mizoguchi K, Soejima A, Unno H (2001) Functional analysis of antibacterial activity of *Bacillus amyloliquefaciens* phage endolysin against Gram-negative bacteria. FEBS Lett 500:56–59

Normark BH, Normark S (2002) Evolution and spread of antibiotic resistance. J Intern Med 252:91–106

Paradis-Bleau C, Cloutier I, Lemieux L, Sanschagrin F, Laroche J, Auger M, Garnier A, Levesque RC (2007) Peptidoglycan lytic activity of the *Pseudomonas aeruginosa* phage phiKZ gp144 lytic transglycosylase. FEMS Microbiol Lett 266:201–209

Picard F, Pezolet M, Bougis PE, Auger M (1996) Model of interaction between a cardiotoxin and dimyristoylphosphatidic acid bilayers determined by solid-state ^{31}P NMR spectroscopy. Biophys J 70:1737–1744

Picard F, Paquet M-J, Levesque J, Belanger A, Auger M (1999) ^{31}P NMR first spectral moment study of the partial magnetic orientation of phospholipid membranes. Biophys J 77:888–902

Pinheiro TJ, Watts A (1994) Resolution of individual lipids in mixed phospholipid membranes and specific lipid-cytochrome c interactions by magic-angle spinning solid-state phosphorus-31 NMR. Biochemistry 33:2459–2467

Polozov IV, Polozova AI, Anantharamaiah GM, Segrest JP, Epand RM (1994) Mixing rates can markedly affect the kinetics of peptide-induced leakage from liposomes. Biochem Mol Biol Int 33:1073–1079

Projan S (2004) Phage-inspired antibiotics? Nat Biotechnol 22:167–168

Pukala TL, Boland MP, Gehman JD, Kuhn-Nentwig L, Separovic F, Bowie JH (2007) Solution structure and interaction of cupiennin

1a, a spider venom peptide, with phospholipid bilayers. Biochemistry 46:3576–3585
Ramamoorthy A (2009) Beyond NMR spectra of antimicrobial peptides: dynamical images at atomic resolution and functional insights. Solid State Nucl Magn Reson 35:201–207
Ramanculov E, Young R (2001) Genetic analysis of the phage T4 holin: timing and topology. Gene 265:25–36
Richard J-A, Kelly I, Marion D, Pezolet M, Auger M (2002) Interaction between β-purothionin and dimyristoylphosphatidylglycerol: a ^{31}P-NMR and infrared spectroscopic study. Biophys J 83:2074–2083
Sao-José C, Parreira R, Vieira G, Santos MA (2000) The N-terminal region of the *Oenococcus oeni* bacteriophage fOg44 lysin behaves as a bona fide signal peptide in *Escherichia coli* and as a cis-inhibitory element, preventing lytic activity on oenococcal cells. J Bacteriol 182:5823–5831
Savitzky A, Golay MJE (1964) Smoothing and differentiation of data by simplified least squares procedures. Anal Chem 36:1627–1639
Seelig J (1978) Phosphorus-31 nuclear magnetic resonance and the head group structure of phospholipids in membranes. Biochim Biophys Acta 515:105–140
Seelig J, Seelig A (1980) Lipid conformation in model membranes and biological membranes. Q Rev Biophys 13:19–61
Sitaram N, Nagaraj R (1993) Interaction of the 47-residue antibacterial peptide seminalplasmin and its 13-residue fragment which has antibacterial and hemolytic activities with model membranes. Biochemistry 32:3124–3130
Smith ICP, Ekiel IH (1984) In: Gorenstein D (ed) Phosphorus-31 NMR of phospholipids in membranes. Phosphorus-31 NMR: Principal applications. Academic Press, London,pp 447–475
Sunhwan J, Vargyas M, Vasko-Szedlar J, Roux M, Im W (2008) PBEQ-Solver for online visualization of electrostatic potential of biomolecules. Nucleic Acids Res 36:W270–W275
Tapanendu K, Pal K, Talapatra GB (2007) Interaction of ovalbumin with phospholipids Langmuir-Blodgett film. J Phys Chem 111:1199–1205
Thiel K (2004) Old dogma, new tricks-21st century phage therapy. Nat Biotechnol 22:31–36
Vitovic P, Kresak S, Naumann R, Schiller SM, Lewis RN, McElhaney RN, Hianik T (2004) The study of the interaction of a model alpha-helical peptide with lipid bilayers and monolayers. Bioelectrochemistry 63:169–176
Volinsky R, Kolusheva S, Berman A, Jelinek R (2004) Microscopic visualization of alamethicin incorporation into model membrane monolayers. Langmuir 20:11084–11091
Volinsky R, Kolusheva S, Berman A, Jelinek R (2006) Investigations of antimicrobial peptides in planar film systems. Biochim Biophys Acta 1758:1393–1407
Watts A, Ulrich AS, Middleton DA (1995) Membrane protein structure: the contribution and potential of novel solid state NMR approaches. Mol Membr Biol 12:233–246
Winsel K, Honig D, Lunkenheimer K, Geggel K, Witt C (2003) Quantitative Brewster angle microscopy of the surface film of human broncho-alveolar lavage fluid. Eur Biophys J 32:544–552
Xu M, Struck DK, Deaton J, Wang I-N, Young R (2004) A signal-arrest-release sequence mediates export and control of the phage P1 endolysin. Proc Natl Acad Sci USA 101:6415–6420
Young R, Wang I-N, Roof WD (2000) Phages will out: strategies of host cell lysis. Trends Microbiol 8:120–128
Zhang YP, Lewis RN, McElhaney RN (1997) Calorimetric and spectroscopic studies of the thermotropic phase behavior of the n-saturated 1, 2-diacylphosphatidylglycerols. Biophys J 72:779–793